Hybrid Materials

DOI: 10.1002/anie.201207448

Immobilization of a Molecular Cobaloxime Catalyst for Hydrogen Evolution on a Mesoporous Metal Oxide Electrode**

*Nicoleta M. Muresan, Janina Willkomm, Dirk Mersch, Yana Vaynzof, and Erwin Reisner**

The sustainable production of H_2 through water splitting faces several fundamental challenges, such as the requirement of a renewable energy input, as well as fast and inexpensive catalysts to minimize energy losses during fuel formation.[1] Finely tuned proton-coupled multi-electron chemistry allows for the formation of H–H and O=O bonds in and from water, which is otherwise inherently slow or requires high electrochemical potentials in the absence of a catalyst.[2] A developing approach in water splitting is the utilization of molecular catalysts integrated onto electrodes to lower the over-potential requirement to drive water oxidation[3] and proton reduction.[4] The heterogenization of molecular catalysts resulted in stimulating discussions about the identity of the true catalyst in the solid-state material. In principle, the immobilized catalyst can either be an active molecular electrocatalyst or simply serve as the precursor for a deposited electroactive metal or metal oxide species.[5]

Cobalt tetraimine complexes[6] are a well-known inexpensive alternative to precious metal catalysts,[7] and therefore receive much attention as inexpensive H_2 evolution catalysts. Cobalt complexes such as $[Co^{III}(dpg)_3(BF)_2](BF_4)]$, $[Co^{III}Cl_2\{(DO)(DOH)pn\}]$ and $[Co^{III}(dmgBF_2)_2(MeCN)_2]$ (Figure 1) were recently used for the preparation of electroactive materials for the reduction of aqueous protons.[8] However, the former two complexes served solely as molecular precursors for the deposition of electroactive Co^0 or CoO_x species,[8a,b] and the latter complex is a precursor for an unknown electroactive catalyst.[8c]

Herein, we report on the synthetic procedure for a novel type of $[Co^{III}Br_2\{(DO)(DOH)pn\}]$ complex ([**Co**]) that features a doubly phosphonated propanediyl bridgehead in the equatorial diimine–dioxime ligand (Figure 1). The phosphonic acid groups provide a strong anchor to metal oxide surfaces,[9] and the robust tetradentate ligand framework provides the cobaloxime with high stability.[6c] Complex [**Co**] was subsequently immobilized on conducting and mesoporous ITO on ITO-coated glass (ITO | *meso*-ITO) with high stability. The nanostructured surface allows for a high loading of [**Co**] on ITO | *meso*-ITO (Scheme 1) and the hybrid electrode exhibits some electrochemical reduction of aqueous protons in a pH-neutral electrolyte solution at room temperature. Limitations of the [**Co**]-modified ITO material arise from electrodegradation of ITO at negative potentials, but a SnO_2 cathode shows improved stability. Finally, spectroelectrochemical investigations and extensive surface characterization confirm that the surface-immobilized cobaloxime [**Co**] remains molecularly intact on the metal oxide electrode after prolonged electrochemical treatment.

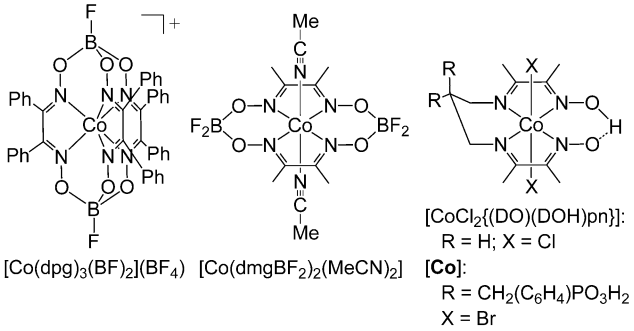

Figure 1. Chemical structures of $[Co^{III}(dpg)_3(BF)_2](BF_4)$,[8a] $[Co^{III}(dmgBF_2)_2(MeCN)_2]$,[6a,8c] $[Co^{III}Cl_2\{(DO)(DOH)pn\}]$,[6c] and the novel cobaloxime [**Co**] with two phosphonic acid anchors for immobilization on a metal oxide surface (this work). $dpgH_2$ = diphenylglyoxime, $dmgH_2$ = dimethylglyoxime, (DO)(DOH)pn = N^2,$N^{2'}$-propanediyl-bis(2,3-butanedione-2-imine-3-oxime).

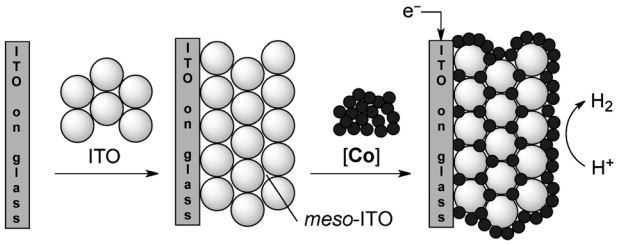

Scheme 1. Illustration of the assembly of a cathode consisting of an ITO conducting glass modified with a *meso*-ITO film and an integrated [**Co**] catalyst (ITO | *meso*-ITO | [**Co**]).

Compound [**Co**] was prepared in six steps, as summarized in Scheme 2, and all compounds were characterized by ^{1}H NMR spectroscopy, ESI-MS, and elemental analysis (see the Supporting Information). The nitrile derivative **2** was

[*] Dr. N. M. Muresan, J. Willkomm, D. Mersch, Dr. E. Reisner
Christian Doppler Laboratory for Sustainable SynGas Chemistry, Department of Chemistry, University of Cambridge
Cambridge CB2 1EW (UK)
E-mail: reisner@ch.cam.ac.uk
Homepage: http://www-reisner.ch.cam.ac.uk/
Dr. Y. Vaynzof
Cavendish Laboratory, University of Cambridge
Cambridge, CB3 0HE (UK)

[**] This work was supported by the U.K. Engineering and Physical Sciences Research Council (EP/H00338X/2), the Austrian Christian Doppler Research Association (Federal Ministry of Economy, Family and Youth, and the National Foundation for Research, Technology and Development) and the OMV Group. We are grateful to Dr. John Davies for his help with X-ray crystallography.

Supporting information for this article is available on the WWW under http://dx.doi.org/10.1002/anie.201207448.

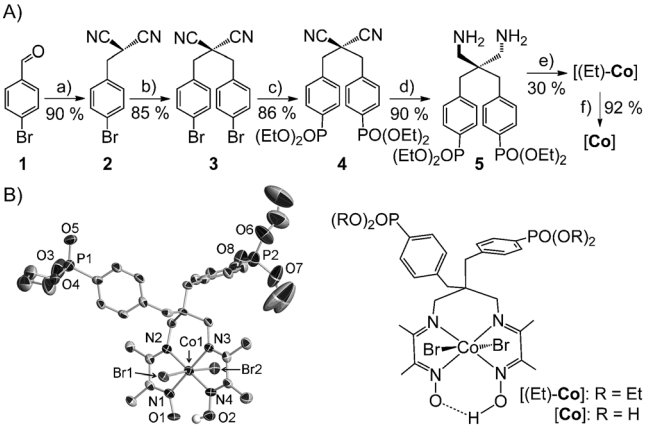

Scheme 2. A) a) Malononitrile, $NaBH_4$, EtOH, RT, 2 h;[10] b) 4-Bromobenzyl bromide, K_2CO_3, acetone, RT, 12 h; c) $HPO(OEt)_2$, NEt_3, Pd-$(PPh_3)_4$, PPh_3, THF, reflux, 48 h; d) BH_3·THF, THF, RT, 12 h; e) 2,3-butanedione monoxime, MeOH, $CoBr_2$·$6H_2O$, RT, 5 d; f) TMSBr, CH_2Cl_2, MeOH, RT, 2 d. B) X-ray crystal structure of [(Et)-**Co**]·2 MeOH with ellipsoids set at the 50% probability level; solvent molecules and hydrogen atoms are omitted for clarity. [(Et)-**Co**]·2 MeOH crystallizes in space group $P\bar{1}$, with the following unit cell parameters: $a = 8.0275(3)$, $b = 14.6652(5)$, $c = 19.8143(7)$ Å and $\alpha = 74.307(2)$, $\beta = 82.998(2)$, $\gamma = 80.199(2)°$; $V = 2205.83(14)$ Å^3. $R_1 = 0.049$. More crystallographic details can be found in the Supporting Information, Tables S1–S3.

synthesized in 90% yield from commercially available malononitrile, 4-bromobenzylaldehyde (**1**), and sodium borohydride.[10] Deprotonation of the methyne proton in **2** with K_2CO_3 allowed for the introduction of a second alkyl chain with 4-bromobenzyl bromide in acetone to give **3** in 85% yield. Compound **3** reacts with diethylphosphite and Pd-$(PPh_3)_4$/PPh_3/NEt_3 in refluxing THF to afford the cross-coupled phosphonate ester **4** in 86% yield. Reduction of nitrile **4** with excess BH_3 at room temperature gives **5** in 90% yield.

Complex [(Et)-**Co**] was prepared by stirring the diamine **5** with two equivalents of 2,3-butanedione monoxime in MeOH for five days at room temperature, followed by complexation with $CoBr_2$·$6H_2O$ and exposure to air for five min. [(Et)-**Co**] was isolated as a green microcrystalline solid and was hydrolyzed to the cobalt phosphonic acid complex [**Co**] in 92% yield by reaction with trimethylsilyl bromide in CH_2Cl_2 at room temperature. Complex [**Co**] was isolated as a green powder and was characterized by ^{1}H, ^{13}C, and ^{31}P NMR spectroscopy, ESI-MS, and elemental analysis. The diamagnetic complexes [**Co**] and [(Et)-**Co**] showed well-defined NMR spectra with a characteristic signal at 19.0 ppm in the ^{1}H NMR spectrum, which was assigned to the equatorial O···H–O bridge protons. The resonance of the bridge methylene protons at 3.0 ppm in **5** is shifted downfield to 3.9 ppm upon complexation to form [(Et)-**Co**] or [**Co**]. The UV/Vis spectrum of [**Co**] in dimethylformamide (DMF) shows one intense absorption at 295 nm ($\varepsilon = 1.9 \times 10^4$ M^{-1}cm^{-1}) and two weak features at 596 nm and 670 nm ($\varepsilon = 33$ and 31 M^{-1}cm^{-1}, respectively). This high-yield synthetic procedure gives access to a range of (DO)(DOH)pn-$(CH_2$-R$)_2$ type ligands with different functional groups at the equatorial bridge position.

Single crystals of [(Et)-**Co**]·2 MeOH suitable for X-ray analysis were obtained by slow evaporation of a concentrated MeOH solution of the complex, and the crystal structure of the complex is depicted in Scheme 2 B. In this structure, complex [(Et)-**Co**] consists of the expected octahedral environment around the cobalt center and two bromido ligands occupying the axial sites [Br1-Co2-Br2, 175.26(3)°]. The two oxime units of the tetradentate ligand join together in the equatorial plane through an intramolecular hydrogen bond [O1···O2, 2.492(6) Å]. The average Co–N (1.91 Å) and Co–Br (2.36 Å) distances are in agreement with the respective bond lengths in related cobaloxime complexes.[6c,11]

Electrochemical measurements of [**Co**] were first recorded on a glassy carbon electrode in DMF with $[N(n\text{Bu})_4]BF_4$ (0.1 M). Cyclic voltammograms (CVs) display the typical[6c,8c] electrochemical response for cobaloximes and show two one-electron reduction waves, which were assigned to the Co^{III}/Co^{II} and Co^{II}/Co^{I} processes at $^{III/II}E_p = 0.01$ V and $^{II/I}E_{1/2} = -0.37$ V vs. NHE (Supporting Information, Figure S1). We note that diimines are potentially redox non-innocent and the two single-electron reductions of [**Co**] could therefore also result in a ligand-based reduction product ($Co^{II}L^{\bullet-}$) instead of Co^{I}.[12] In the presence of trifluoroacetic acid (TFA; $pK_a = 6$ in DMF),[13] an electrocatalytic proton reduction wave is observed at a potential close to the Co^{II}/Co^{I} couple. The observed overpotential of approximately 250 mV (Figure S1) is in agreement with previous reports for Co–tetraimine complexes.[14] Thus, the catalytic core of [**Co**] is fully active upon functionalization of the (DO)(DOH)pn ligand.

The presence of the phosphonic acid moiety in [**Co**] provides the complex with high solubility in water. The CV of [**Co**] in an aqueous TEOA/Na_2SO_4 (TEOA = triethanolamine; 0.1 M each) solution at pH 7 and 25 °C at a planar (2D) ITO electrode displays two one-electron reduction waves, which were assigned to Co^{III}/Co^{II} and Co^{II}/Co^{I} processes at $^{III/II}E_p = -0.20$ V and $^{II/I}E_p = -0.53$ V vs. NHE at a scan rate of 100 mV s^{-1} (Figure S2). The catalytic onset reduction potential is observed at E_{cat} of approximately −0.72 V vs. NHE; at an overpotential of approximately 0.3 V at pH 7 ($E^{0\prime}_{H+/H2} = -0.42$ vs. NHE).

Subsequently, we prepared ITO | *meso*-ITO electrodes as substrates for the immobilization of [**Co**]. The electrodes were prepared by spreading a suspension of ITO nanoparticles (< 40 nm diameter) on ITO-coated glass slides followed by annealing at 350 °C (Scheme 1).[3a,e] The geometrical *meso*-ITO area was 0.25 cm^2, with a thickness of 13 μm (Figure S3). The ITO | *meso*-ITO working electrodes were then modified with the catalyst by exposing the films to a 6 mM solution of [**Co**] in DMF or an aqueous TEOA/Na_2SO_4 solution (pH 7). The attachment of [**Co**] to *meso*-ITO is not electrochemically assisted, but the adsorption process can be monitored by the increase in current of the Co^{III}/Co^{II} redox couple by running continuous voltammetric cycles (Figure 2 A, inset). Immobilization was completed within two hours in DMF and ten hours in aqueous TEOA solution. CVs and differential pulse voltammograms (DPVs) of an ITO | *meso*-ITO | [**Co**] electrode in TEOA/Na_2SO_4 solution at pH 7 show two one-electron irreversible reduction waves at

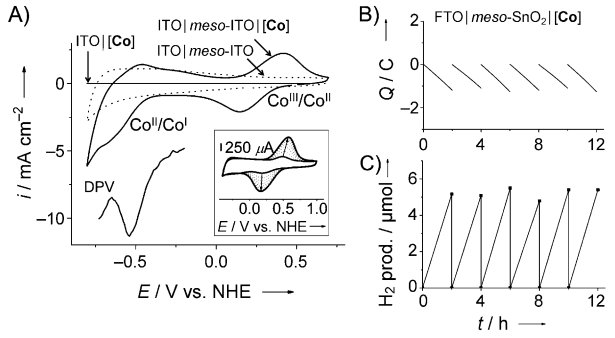

Figure 2. Electrochemistry of [**Co**] in TEOA/Na_2SO_4 solution (0.1 M each, pH 7) at 25 °C. A Ag/AgCl reference, a platinum wire or glassy carbon rod counter, and an ITO, ITO | *meso*-ITO, or FTO | *meso*-SnO_2 working electrode with a scan rate of 100 mV s^{-1} were employed in all experiments. A) CV and DPV (10 mV step potential) of the ITO | *meso*-ITO | [**Co**] electrode, and a control experiment for ITO | *meso*-ITO in the absence of [**Co**], as well as a CV with [**Co**] adsorbed on planar ITO (ITO | [**Co**] with no [**Co**] in solution), for comparison. Inset: Consecutive CVs of an ITO | *meso*-ITO electrode (0.25 cm^2) immersed in an aqueous TEOA/Na_2SO_4 solution containing [**Co**] (6 mM) at 25 °C, showing the increase in the loading of ITO | *meso*-ITO with [**Co**] with time (first scan after 1 min and last scan after approximately 1 h); B) and C) Controlled potential electrolysis at −0.7 V vs. NHE with [**Co**] in solution (0.18 mM) at an FTO | *meso*-SnO_2 working electrode for six two-hour intervals. H_2 was detected in the headspace by gas chromatography with an airtight electrochemical cell.

$^{III/II}E_P = 0.14$ V and $^{II/I}E_P = -0.54$ V vs. NHE at a scan rate of 100 mV s^{-1} (Figures 2 A and S4). CVs in the absence of TEOA or Na_2SO_4 show an identical voltammetric response and both components are therefore innocent in our experiments (Figure S5).

The amount of [**Co**] on the ITO | *meso*-ITO surface was determined by measuring the absorbance difference of the catalyst solution before and after exposure to the *meso*-ITO electrode. The absorbance at 596 nm was used to quantify the loading of the catalyst on the *meso*-ITO electrode (Figure S6). A large loading of (0.030 ± 0.002) mg of [**Co**] on ITO | *meso*-ITO ($\Gamma_0 = $ ca. 1.50×10^{-7} mol cm^{-2}) was obtained from DMF and TEOA/Na_2SO_4 solutions. An ideal monolayer on a 2D surface would allow for only approximately $\Gamma_0 = $ ca. 3×10^{-10} mol cm^{-2} assuming that one molecule of [**Co**] occupies 6 nm^2 on a surface (estimated from the X-ray molecular structure of [(Et)-**Co**]). The high [**Co**] loading on ITO | *meso*-ITO resulted in a current density of 3.7 mA cm^{-2} at −0.7 V vs. NHE (background subtracted) during CV scans in TEOA/Na_2SO_4 (0.1 M, pH 7) solution with a scan rate of 100 mV s^{-1}. An ITO | [**Co**] electrode ([**Co**] adsorbed on planar ITO, no [**Co**] in solution) showed only a current density of 0.014 mA cm^{-2} under the same conditions. Thus, the 3D environment in *meso*-ITO enhances the [**Co**] loading by more than two orders of magnitude, which is in agreement with previously reported values for the integration of a ruthenium complex in *meso*-ITO.[3a]

The increase in current density at −0.7 V vs. NHE in Figure 2 is partially attributed to electrochemical proton reduction in the aqueous pH 7 electrolyte solution.[6d] A closed cell allowed us to detect the formation of some H_2 in the gas headspace by gas chromatography using a thermal conductivity detector during bulk electrolysis with ITO | *meso*-ITO | [**Co**] in TEOA buffer at pH 7, at an applied potential of −0.7 V vs. NHE. However, a disadvantage of ITO is its degradation at negative potentials,[15] and we therefore determined the Faraday efficiency and turnover numbers for electrocatalytic H_2 evolution using a more robust electrode material. Mesoporous SnO_2 on FTO-coated glass (FTO | *meso*-SnO_2; FTO = fluoride-doped tin oxide) was prepared from SnO_2 nanoparticles (< 100 nm diameter; Figure S3) in analogy to ITO | *meso*-ITO electrodes (see the Supporting Information). FTO | *meso*SnO_2 is a low-cost alternative to ITO-based electrodes and displays enhanced stability at negative potentials.

A closed and stirred electrochemical cell containing an aqueous TEOA/Na_2SO_4 solution at pH 7 with [**Co**] (0.18 mM) was poised at a potential of −0.7 V vs. NHE with an FTO | *meso*-SnO_2 electrode (0.5 cm^2, thickness of 13 μm; Figure S3) for two hours. The passage of an average of −1.2 C of charge resulted in 5.3 μmol headspace H_2 (Figures 2 and S7), which corresponds to a high Faraday yield of (87 ± 4)% for dissolved [**Co**]. No H_2 was detected in the headspace after electrolysis without [**Co**]. Extended controlled potential electrolysis (−0.7 V vs. NHE) over 12 h of the same [**Co**] system resulted in the passage of 7.2 C of charge and an accumulation of approximately 32 μmol of H_2 in the headspace, which corresponds to a cobalt-based turnover number of (12 ± 2) mol H_2 (per mol [**Co**]). We note that this number is the lower limit, because [**Co**] was still active after this time and we took into account all of the [**Co**] from the bulk solution. The current density remained constant (ca. 240 μA cm^{-2}) for several hours during electrolysis, thereby confirming the catalytic formation of H_2 at a relatively low overpotential of approximately 0.3 V (Figure 2). Degradation of FTO | *meso*SnO_2 | [**Co**] was only observed after three days of electrolysis, when the deposition of a black layer (presumably metallic Co)[8a] started to appear on the working electrode.

The high [**Co**] loading and the optical transparency of *meso*-ITO allowed us to study the identity and stability of the molecular catalyst on the ITO | *meso*-ITO surface in more detail. Scanning towards negative potentials in DMF or TEOA/Na_2SO_4 with a partially [**Co**]-loaded ITO | *meso*-ITO electrode, allowed for the observation of a color change of adsorbed [**Co**] from yellowish green to red at the Co^{III}/Co^{II} redox potential, and to deep blue following the reduction of the Co^{II} species (Figure 3). The potential-dependent color changes are fully reversible during multiple CV scans and were investigated by transmission UV/Vis spectroelectrochemistry. Electronic absorption spectra for the Co^{III}, Co^{II}, and Co^{I} species were recorded for ITO | *meso*-ITO | [**Co**] in DMF containing $[N(nBu)_4]BF_4$ (0.10 M) at +0.60, −0.10, and −0.60 V vs. NHE with absorbance maxima, λ_{max}, at 450, 507, and 655 nm, respectively (Figure 3 B, red traces). Comparable spectroelectrochemical absorption spectra of the Co^{III}, Co^{II}, and Co^{I} species with ITO | *meso*-ITO | [**Co**] were recorded in TEOA/Na_2SO_4 solution (Figure S8).

The spectroelectrochemical response of ITO | *meso*-ITO | [**Co**] is in agreement with electronic absorption spectra of chemically reduced [**Co**] in DMF. Exposure of $[\mathbf{Co}]^{III}$ to one and two equivalents of cobaltocene (reduction potential is

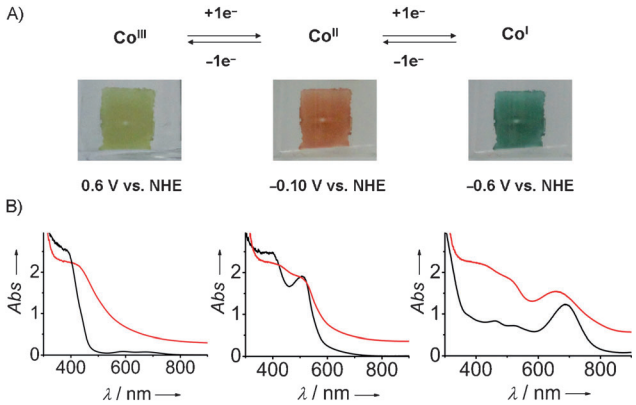

Figure 3. A) The immobilized catalyst [**Co**] is reduced reversibly on *meso*-ITO in two one-electron reduction processes from $Co^{III} \rightarrow Co^{II} \rightarrow Co^{I}$. The pictures of ITO | *meso*-ITO | [**Co**] electrodes were taken during electrochemical experiments in anhydrous DMF containing [N-(nBu)$_4$]BF_4 (0.1 M) at an applied potential of 0.60 V (left), −0.10 V (middle) and −0.60 V (right). B) The corresponding electronic absorption spectra of $[Co]^{III}$, $[Co]^{II}$, and $[Co]^{I}$ in DMF on the ITO | *meso*-ITO electrode (——) and chemically reduced $[Co]^{III}$, $[Co]^{II}$, and $[Co]^{I}$ in solution (——). See text for details.

−0.7 vs. NHE)[16] resulted in the formation of $[Co]^{II}$ and $[Co]^{I}$, respectively (Figures 3B and S9). The UV/Vis spectra showed an absorption maximum at 445 nm ($\varepsilon = 1.55 \times 10^3\,M^{-1}cm^{-1}$) for $[Co]^{III}$, 505 nm ($\varepsilon = 2.4 \times 10^2\,M^{-1}cm^{-1}$) for $[Co]^{II}$, and 680 nm ($\varepsilon = 1.9 \times 10^2\,M^{-1}cm^{-1}$) for $[Co]^{I}$. The UV/Vis spectra are also in agreement with previous spectroscopic data in solution for reduced cobaloxime species,[6a,17] and no particle formation became apparent during chemical reduction. The agreement between spectroscopic data of [**Co**] in solution and on ITO | *meso*-ITO confirms that the majority of the cobaloxime is intact on the electrode surface, even at low potential and over multiple scanning cycles.

The stability of the ITO | *meso*-ITO | [**Co**] electrode was studied by spectroelectrochemistry in DMF and aqueous TEOA/Na_2SO_4 solution. The electrode was immersed in a fresh DMF solution and no spectroscopic or voltammetric change was observed over a period of six hours (Figure S10). The stability of the electrochemically reduced $[Co]^{II}$ (at −0.10 V vs. NHE) and $[Co]^{I}$ (at −0.60 V vs. NHE) on an ITO | *meso*-ITO electrode in dry DMF were also monitored (Figure S11). Electronic absorption spectra show a high stability on the surface with negligible or small leaching into the bulk solution within one hour for the Co^{II} and Co^{I} species, respectively. Analogous experiments were performed with ITO | *meso*-ITO | [**Co**] in an aqueous TEOA/Na_2SO_4 solution and no desorption was observed for [**Co**] (no potential applied) after six hours (Figure S12). Electrochemically generated $[Co]^{II}$ (−0.10 V vs. NHE) disappeared over a period of three hours from the ITO | *meso*-ITO | [**Co**] electrode with a concomitant coloration of the solution with an absorption maximum at 505 nm, which was assigned to intact, but desorbed $[Co]^{II}$ (Figure S13B). The absorption band at 655 nm of the electrochemically generated $[Co]^{I}$ on ITO | *meso*-ITO disappeared after several seconds (Figure S14), presumably because of catalytic turnover and H_2 formation. Scanning towards positive potential after reversal at −0.7 V in TEOA/Na_2SO_4 displayed the genuine $Co^{III/II}$ redox couple at $^{III/II}E_P = 0.14$ V, thus demonstrating that the majority of [**Co**] is neither decomposed nor desorbed from the electrode surface when forming the catalytically active Co^{I} species. The cobalt catalyst can be at least partially desorbed from ITO | *meso*-ITO | [**Co**] when phosphate (1 mL, 25 mM) is added to the TEOA/Na_2SO_4 electrolyte solution during voltammetric experiments (Figure S15), which supports the strong and reversible binding of molecular [**Co**] on ITO through the phosphonic acid anchors.

We subsequently investigated the [**Co**]-modified electrode surfaces by scanning electron microscopy (SEM), energy dispersive X-ray (EDX) and X-ray photoemission spectroscopy (XPS). SEM and EDX analysis before and after controlled potential electrolysis at −0.7 V vs. NHE for 12 h in an aqueous TEOA solution at pH 7 did not reveal significant changes in surface morphology or elemental composition, or the formation of CoO_x or metallic Co particles on *meso*-ITO or planar ITO (Figure S16 and S17).

XPS analysis on ITO | *meso*-ITO | [**Co**] before performing electrochemical experiments in DMF shows the expected spectra for the cobaloxime immobilized on ITO (Figure S18): A Co_{2p} doublet at binding energies of 781.4 eV and 796.4 eV for Co^{III},[18] a Br_{3d} doublet at binding energies of 68.8 eV and 69.7 eV, a P_{2p} doublet at 133.0 eV and 134.2 eV, and two N_{1s} singlet peaks at 399.9 eV and 401.4 eV in a 1:1 ratio for N−C and N−O, respectively. The C_{1s} spectrum consists of two peaks at 284.9 eV (C−C) and 285.9 eV (C−N). In_{3d}, Sn_{3d}, and O_{1s} peaks from *meso*-ITO were also observed. XPS gave almost identical results for ITO | *meso*-ITO | [**Co**] in aqueous TEOA solution, but the bromides were not observed in the Br_{3d} spectrum, presumably owing to their replacement by aqua ligands (Figure S19).

XPS measurements on ITO | *meso*-ITO | [**Co**] after four hours of continuous redox cycling (from −0.8 V to 0.7 V vs. NHE; Figure S20) and after 12 h of controlled potential electrolysis at −0.7 V vs. NHE (Figure S21) in TEOA solution gave comparable results. The P_{2p} and C_{1s} signals in [**Co**] and In_{3d} and Sn_{3d} for the ITO substrate remained unchanged (±0.2 eV) compared to XPS spectra recorded before electrochemical treatment. The N_{1s} spectrum shows an unchanged peak for N−C at 399.9 eV, but a small shift to lower binding energies (400.7 eV) was observed for N−O after CV and chronoamperometry. The shift could be due to partial protonation of the oxygen atom. The Co_{2p} doublet peaks at 781.3 eV and 796.8 eV after electrochemical treatment are accompanied by an additional strong satellite feature at 786.1 eV. The satellite and increased multiplet splitting are indicative of a Co^{II} oxidation state.[18]

XPS analysis of ITO | *meso*-ITO | [**Co**] therefore further supports that a molecular compound is present on the metal oxide and no indication for the formation of CoO_x or metallic Co particles on *meso*-ITO was obtained after several hours of redox cycling or electrolysis. Our results are in agreement with a recent report, where no cobalt-containing nanoparticles were formed from [$CoCl_2${(DO)(DOH)pn}] on FTO at −0.7 V vs. NHE.[8b] XPS analysis of FTO | *meso*-SnO_2 | [**Co**] was not possible, owing to the low conductivity of SnO_2 relative to ITO. However, XPS analysis of a planar FTO

electrode modified with [**Co**] (and [**Co**] in solution) after 12 h of controlled potential electrolysis at −0.7 V vs. NHE in TEOA solution gave comparable results to ITO | *meso*-ITO | [**Co**] and showed the presence of the molecular cobalt catalyst on FTO.

In summary, we have presented the rational assembly of a hybrid electrode with a novel cobaloxime complex immobilized on *meso*-ITO. The high yielding method of [**Co**] preparation gives access to a new strategy for the functionalization of the propanediyl-bridge of the (DO)(DOH)pn ligand. The [**Co**] complex contains two phosphonic acid linkers to guarantee strong attachment to a metal oxide surface, and the equatorial diimine–dioxime ligand framework allows for high stability of the catalyst on the electrode. The mesoporous ITO surface allows for high catalyst loadings and the ITO | *meso*-ITO | [**Co**] electrode shows high current densities and some electrochemical proton reduction in pH 7 aqueous solution. We investigated the molecular nature of the catalyst by spectroelectrochemistry, SEM, EDX, and XPS analysis. Our spectroelectrochemical studies demonstrate that a molecular Co catalyst is intact on the electrode surface even when applying moderately negative potentials. The solid-state characterization techniques did not reveal the formation of Co-containing nanoparticles or other decomposition products of [**Co**] during several hours of electrocatalytic H_2 formation. Our approach to integrate molecular H_2 evolution catalysts with nanostructured materials might ultimately give access to robust and highly active electrodes for water splitting. Work is currently in progress to overcome limitations from the electrodegradation of ITO at low potentials by exploring more robust electrode materials, and to extend this work to hybrid materials with other molecular catalysts.

Received: September 14, 2012
Published online: November 21, 2012

Keywords: cobalt · heterogeneous catalysis · hybrid materials · proton reduction · water splitting

[1] a) S. Y. Reece, J. A. Hamel, K. Sung, T. D. Jarvi, A. J. Esswein, J. J. H. Pijpers, D. G. Nocera, *Science* **2011**, *334*, 645 – 648; b) Q. Yin, J. M. Tan, C. Besson, Y. V. Geletii, D. G. Musaev, A. E. Kuznetsov, Z. Luo, K. I. Hardcastle, C. L. Hill, *Science* **2010**, *328*, 342 – 345; c) S. W. Kohl, L. Weiner, L. Schwartsburd, L. Konstantinovski, L. J. W. Shimon, Y. Ben-David, M. A. Iron, D. Milstein, *Science* **2009**, *324*, 74 – 77; d) N. Armaroli, V. Balzani, *Angew. Chem.* **2007**, *119*, 52 – 67; *Angew. Chem. Int. Ed.* **2007**, *46*, 52 – 66; e) Y. Tachibana, L. Vayssieres, J. R. Durrant, *Nat. Photonics* **2012**, *6*, 511 – 518.

[2] a) F. A. Armstrong, J. Hirst, *Proc. Natl. Acad. Sci. USA* **2011**, *108*, 14049 – 14054; b) J. K. Nørskov, J. Rossmeisl, A. Logadottir, L. Lindqvist, J. R. Kitchin, T. Bligaard, H. Jonsson, *J. Phys. Chem. B* **2004**, *108*, 17886 – 17892; c) W. Sheng, H. A. Gasteiger, Y. Shao-Horn, *J. Electrochem. Soc.* **2010**, *157*, B1529 – B1536; d) S. Hammes-Schiffer, *Acc. Chem. Res.* **2009**, *42*, 1881 – 1889.

[3] a) P. G. Hoertz, Z. Chen, C. A. Kent, T. J. Meyer, *Inorg. Chem.* **2010**, *49*, 8179 – 8181; b) K. Hanson, M. K. Brennaman, A. Ito, H. Luo, W. Song, K. A. Parker, R. Ghosh, M. R. Norris, C. R. K. Glasson, J. J. Concepcion, R. Lopez, T. J. Meyer, *J. Phys. Chem. C* **2012**, *116*, 14837 – 14847; c) C. R. K. Glasson, W. Song, D. L. Ashford, A. Vannucci, Z. Chen, J. J. Concepcion, P. L. Holland, T. J. Meyer, *Inorg. Chem.* **2012**, *51*, 8637 – 8639; d) K. S. Joya, N. K. Subbaiyan, F. D'Souza, H. J. M. d. Groot, *Angew. Chem.* **2012**, *124*, 9739 – 9743; *Angew. Chem. Int. Ed.* **2012**, *51*, 9601 – 9605; e) M. Kato, T. Cardona, A. W. Rutherford, E. Reisner, *J. Am. Chem. Soc.* **2012**, *134*, 8332 – 8335; f) F. Li, B. Zhang, X. Li, Y. Jiang, L. Chen, Y. Li, L. Sun, *Angew. Chem.* **2011**, *123*, 12484 – 12487; *Angew. Chem. Int. Ed.* **2011**, *50*, 12276 – 12279; g) L. Tong, M. Göthelid, L. Sun, *Chem. Commun.* **2012**, *48*, 10025 – 10027; h) R. Brimblecombe, A. Koo, G. C. Dismukes, G. F. Swiegers, L. Spiccia, *J. Am. Chem. Soc.* **2010**, *132*, 2892 – 2894.

[4] a) T. Nann, S. K. Ibrahim, P.-M. Woi, S. Xu, J. Ziegler, C. J. Pickett, *Angew. Chem.* **2010**, *122*, 1618 – 1622; *Angew. Chem. Int. Ed.* **2010**, *49*, 1574 – 1577; b) A. Le Goff, V. Artero, B. Jousselme, P. D. Tran, N. Guillet, R. Métayé, A. Fihri, S. Palacin, M. Fontecave, *Science* **2009**, *326*, 1384 – 1387; c) L. R. Webster, S. K. Ibrahim, J. A. Wright, C. J. Pickett, *Chem. Eur. J.* **2012**, *18*, 11798 – 11803.

[5] a) U. Hintermair, S. M. Hashmi, M. Elimelech, R. H. Crabtree, *J. Am. Chem. Soc.* **2012**, *134*, 9785 – 9895; b) J. J. Stracke, R. G. Finke, *J. Am. Chem. Soc.* **2011**, *133*, 14872 – 14875.

[6] a) X. Hu, B. S. Brunschwig, J. C. Peters, *J. Am. Chem. Soc.* **2007**, *129*, 8988 – 8998; b) S. Losse, J. G. Vos, S. Rau, *Coord. Chem. Rev.* **2010**, *254*, 2492 – 2504; c) P. A. Jacques, V. Artero, J. Pecaut, M. Fontecave, *Proc. Natl. Acad. Sci. USA* **2009**, *106*, 20627 – 20632; d) C. C. L. McCrory, C. Uyeda, J. C. Peters, *J. Am. Chem. Soc.* **2012**, *134*, 3164 – 3170; e) V. Artero, M. Chavarot-Kerlidou, M. Fontecave, *Angew. Chem.* **2011**, *123*, 7376 – 7405; *Angew. Chem. Int. Ed.* **2011**, *50*, 7238 – 7266; f) J. L. Dempsey, B. S. Brunschwig, J. R. Winkler, H. B. Gray, *Acc. Chem. Res.* **2009**, *42*, 1995 – 2004; g) P. Connolly, J. H. Espenson, *Inorg. Chem.* **1986**, *25*, 2684 – 2688; h) F. Lakadamyali, M. Kato, N. M. Muresan, E. Reisner, *Angew. Chem.* **2012**, *124*, 9515 – 9518; *Angew. Chem. Int. Ed.* **2012**, *51*, 9381 – 9384.

[7] D. V. Esposito, S. T. Hunt, A. L. Stottlemyer, K. D. Dobson, B. E. McCandless, R. W. Birkmire, J. G. Chen, *Angew. Chem.* **2010**, *122*, 10055 – 10058; *Angew. Chem. Int. Ed.* **2010**, *49*, 9859 – 9862.

[8] a) E. Anxolabéhère-Mallart, C. Costentin, M. Fournier, S. Nowak, M. Robert, J.-M. Savéant, *J. Am. Chem. Soc.* **2012**, *134*, 6104 – 6107; b) S. Cobo, J. Heidkamp, P.-A. Jacques, J. Fize, V. Fourmond, L. Guetaz, B. Jousselme, V. Ivanova, H. Dau, S. Palacin, M. Fontecave, V. Artero, *Nat. Mater.* **2012**, *11*, 802 – 807; c) L. A. Berben, J. C. Peters, *Chem. Commun.* **2010**, *46*, 398 – 400.

[9] C. Queffélec, M. Petit, P. Janvier, D. A. Knight, B. Bujoli, *Chem. Rev.* **2012**, *112*, 3777 – 3807.

[10] F. Tayyari, D. E. Wood, P. E. Fanwick, R. E. Sammelson, *Synthesis* **2008**, *2*, 279 – 285.

[11] a) M. Giorgetti, M. Berrettoni, I. Ascone, S. Zamponi, R. Seeber, R. Marassi, *Electrochim. Acta* **2000**, *45*, 4475 – 4482; b) F. Lakadamyali, E. Reisner, *Chem. Commun.* **2011**, *47*, 1695 – 1697.

[12] a) O. Pantani, E. Anxolabéhère-Mallart, A. Aukauloo, P. Millet, *Electrochem. Commun.* **2007**, *9*, 54 – 58; b) N. Muresan, K. Chlopek, T. Weyhermüller, F. Neese, K. Wieghardt, *Inorg. Chem.* **2007**, *46*, 5327 – 5337.

[13] V. Fourmond, S. Canaguier, B. Golly, M. J. Field, M. Fontecave, V. Artero, *Energy Environ. Sci.* **2011**, *4*, 2417 – 2427.

[14] V. Fourmond, P.-A. Jacques, M. Fontecave, V. Artero, *Inorg. Chem.* **2010**, *49*, 10338 – 10347.

[15] P. M. S. Monk, *Fundamentals of Electroanalytical Chemistry*, Wiley, Kent, UK, **2002**.

[16] N. G. Connelly, W. G. Geiger, *Chem. Rev.* **1996**, *96*, 877 – 910.

[17] T. Lazarides, T. McCormick, P. Du, G. Luo, B. Lindley, R. Eisenberg, *J. Am. Chem. Soc.* **2009**, *131*, 9192 – 9194.

[18] T. J. Chuang, C. R. Brundle, D. W. Rice, *Surf. Sci.* **1976**, *59*, 413 – 429.

